Received: 10 May 2023 | Revised: 14 July 2023 | Accepted: 11 August 2023

DOI: 10.1002/nbm.5032

RESEARCH ARTICLE

NMR IN BIOMEDICINE WILEY

The impact of variations in subject geometry, respiration and coil repositioning on the specific absorption rate in parallel transmit abdominal imaging at 7 T

Emma Doran[1,2] | Iyad Naim[1] | Richard Bowtell[1] | Penny A. Gowland[1] | Paul M. Glover[1] | Stephen Bawden[1,3]

[1]Sir Peter Mansfield Imaging Centre, School of Physics and Astronomy, University of Nottingham, Nottingham, UK

[2]Department of Clinical Physics and Bioengineering, NHS Greater Glasgow & Clyde, Glasgow, UK

[3]NIHR Nottingham Biomedical Research Centre, Nottingham University Hospitals NHS Trust, University of Nottingham, Nottingham, UK

Correspondence
Stephen Bawden, Sir Peter Mansfield Imaging Centre, School of Physics and Astronomy, University of Nottingham, Nottingham NG7 2RD, UK.
Email: stephen.bawden@nottingham.ac.uk

Funding information
EPSRC/MRC Oxford Nottingham Biomedical Imaging Centre for Doctoral Training; MRC Clinical Research Capabilities & Technologies Initiative Award

Abstract

Parallel transmit MRI at 7 T has increasingly been adopted in research projects and provides increased signal-to-noise ratios and novel contrasts. However, the interactions of fields in the body need to be carefully considered to ensure safe scanning. Recent advances in physically flexible body coils have allowed for high-field abdominal imaging, but the effects of increased variability on energy deposition need further exploration. The aim of this study was to assess the impact of subject geometry, respiration phase and coil positioning on the specific absorption rate (SAR). Ten healthy subjects (body mass index [BMI] $= 25 \pm 5$ kg m^{-2}) were scanned (at 3 T) during exhale breath-hold and images used to generate body models. Seven of these subjects were also scanned during inhale. Simplifications of the coil and body models were first explored, and then finite-difference time-domain simulations were run with a typical eight-channel parallel transmit coil positioned over the abdomen. Simulations were used to generate 10 g averaged SAR (SAR_{10g}) maps across 100,000 phase settings, and the worst-case scenario 10 g averaged SAR ($wocSAR_{10g}$) was identified using trigonometric maximisation. The average maximum SAR_{10g} across the 10 subjects with 1 W input power per channel was 1.77 W kg^{-1}. Hotspots were always close to the body surface near the muscle wall boundary. The $wocSAR_{10g}$ across the 10 subjects ranged from 2.3 to 3.2 W kg^{-1} and was inversely correlated to fat volume percentage ($R = 8$) and BMI ($R = 0.6$). The coefficient of variation values in SAR_{10g} due to variations in subject geometry, respiration phase and realistic coil repositioning were 12%, 4% and 12%, respectively. This study found that the variability due to realistic coil repositioning was similar to the variability due to differing healthy subject geometries for abdominal imaging. This is important as it suggests that population-based modelling is likely to be more useful than individual modelling in setting safe thresholds for abdominal imaging.

Abbreviations: FDTD, finite difference time domain; MIP, maximum intensity projection; SAR, specific absorption rate; SAR_{10g}, 10 g averaged specific absorption rate; SNR, signal-to-noise ratio; VOP, virtual observation point; $wocSAR_{10g}$, worst-case scenario 10 g averaged specific absorption rate.

KEYWORDS
abdominal imaging, finite element electromagnetic modelling, high-field MRI, parallel transmit, specific absorption rate

1 | INTRODUCTION

Abdominal MR imaging at 7 T promises increased signal-to-noise ratio (SNR) and access to novel contrasts.[1,2] However, the short wavelength of radio frequency (RF) magnetic fields in human tissues at 7 T leads to significant interference inside the body so that abdominal MR imaging (MRI) requires the use of parallel RF transmit technology to ensure that adequate and homogeneous B_1^+ can be generated in target organs.[3] Various RF coil designs have been proposed[4–6] with the dipole antenna[7] showing significant advantages for imaging deep tissue. A minimum separation between transmit elements is required for adequate decoupling and most MR systems that are equipped with parallel transmit technology only have a limited number of channels. These factors have led to the quite widespread adoption of the eight-channel parallel transmit dipole array with flat-plate, meandered elements for 7-T abdominal MRI.[3,8,9] However, the RF power required for excitation increases with field strength, and this energy is deposited more inhomogeneously within the body compared with lower field strengths due to interference of the RF field within the tissues[10,11] and the coupling of the transmit coils. Therefore, global specific absorption rate (SAR) and local SAR distributions must be determined for each subject to ensure that safety restrictions are met.[12,13]

At lower resonant frequencies, electromagnetic (EM) field distributions can be modelled using analytical methods with static field approximations.[14] However, these approximations are not valid at higher frequencies as the wavelength approaches the size of the sample, and full EM finite-difference time-domain (FDTD) numerical simulations are required.[15] These methods are challenging, with special attention needed to ensure robust and accurate simulations.[16,17] They also place a high demand on computer resources and simulation time due to the level of detail of the coil and tissue model, the multiple RF sources used in parallel transmit and the iterative nature of FDTD simulations.

In order to estimate SAR from EM FDTD simulations in a parallel transmit system, the interactions between the fields from different transmit elements must be considered, taking account of their relative amplitudes and phases.[16] While in systems with geometrically fixed transmit elements, such as head coils, the spatial variation in the relative phase of each transmitted field can be readily known, the mechanical flexibility of body coils makes the transmitted field less predictable. As a result, it is common to set safety limits for abdominal coils by simulating the E fields for a range of subject geometries and determining the distribution in SAR for equal input power per channel (e.g., 1 W) across possible variations in phase settings. From this, a maximum power limit per channel can be set on the scanner, below which the simulations predict that SAR remains within safe limits.[11,18,19]

There are a number of other sources of variability that may impact the SAR when using flexible parallel transmit body coils for abdominal imaging at 7 T. Firstly, variability in the subject's tissue geometry and EM properties will result in varying field interactions leading to varying patterns of energy deposition. Previous work has investigated this intersubject variability in prostate scanning[20] and found that worst-case local SAR ranged from 2.6 to 4.6 W kg^{-1} for an input power of 1 W per channel. Secondly, respiration can cause relative movement between the coil and subject, and varying field interactions within the lungs and at lung–tissue boundaries, which are likely to result in intrasubject variability in SAR across time. Schoen et al.[21] investigated respiration effects in cardiac imaging where the effects of lung volume are the most pronounced and found a significant impact on the B_1^+ distribution and maximum local SAR. Finally, as opposed to fixed coils (e.g., a parallel transmit head coil), a body coil is conformed to the body shape, with the exact location being chosen by the scanner operators. This will result in shifts in relative coil position from one scan to another.

The aim of this study was to develop a simplified modelling regime for parallel transmit abdominal imaging at 7 T and use it to assess the effects of variability in subject geometry, respiration and coil positioning on SAR.

2 | METHODS

Ethical approval was granted for MRI scanning by the local ethics committee. All participants were screened for eligibility and MR safety, and informed consent was obtained.

EM simulations were performed in Remcom XFdtd 7.7.1[22] using an NVIDIA Titan Xp GPU, with a minimum feature size of five cells for good conductors and two cells for poor conductors, resulting in minimum cell edge lengths of $3.6 \times 1.5 \times 0.4$ mm^3 around the dipole feeds and maximum edge lengths of $7.8 \times 7.7 \times 29.2$ mm^3 towards the periphery of the simulation space.

The simulation space was modelled using Cartesian *ProGrid* meshing (20 vs. 10 minimum cells per wavelength for regions of good vs. poor conductors, respectively). Remcom's non-Cartesian subcellular conformal meshing (XACT) was used on the full meandered model for methodology validation (see below). Throughout this work, the EM properties of tissues were assigned according to the Remcom tissue library (Table 1).

TABLE 1 Simulated maximum SAR_{10g} for successively simplified models and tissue conductivity and density values.

Model type (lung tissue conductivity and density is assigned throughout all models)	Mean ± standard deviation of max SAR_{10g} for 100,000 phase settings (W kg^{-1})		Absolute max SAR_{10g} across all 100,000 phase settings (W kg^{-1})	
	Male	Female	Male	Female
Full (organ specific)*	1.7 ± 0.2	1.4 ± 0.2	2.7	2.2
Organs as muscle	1.6 ± 0.2	1.4 ± 0.2	2.4	2.2
Organs as muscle, bone as fat	1.7 ± 0.2	1.4 ± 0.2	2.8	2.2
Organs and skin as muscle	1.5 ± 0.2	1.4 ± 0.2	3.3	3.3
Organ as muscle, skin as fat	2.2 ± 0.2	2.1 ± 0.3	2.6	2.4
Organ as muscle, skin and bone as fat	1.5 ± 0.2	1.3 ± 0.2	2.6	2.5

Abbreviation: max SAR_{10g}, maximum 10 g averaged specific absorption rate.

Tissue conductivity (σ) and density (ρ) values (from Remcom's tissue library):

	σ (S m^{-1})	ρ (kg m^{-3})		σ (S m^{-1})	ρ (kg m^{-3})		σ (S m^{-1})	ρ (kg m^{-3})
Gallbladder	*1.1*	*1071*	*Lung*	*0.4*	*294*	*Bone*	*0.2*	*1178*
Heart	*1*	*1081*	*Small intestines*	*1.8*	*1030*	*Fat*	*0.08*	*911*
Kidney	*1*	*1066*	*Spleen*	*1*	*1089*	*Muscle*	*0.8*	*1090*
Liver	*0.6*	*1079*	*Stomach*	*1*	*1088*	*Skin*	*0.6*	*1109*

Open boundary conditions were defined in all directions, and calculations were terminated with a system energy decay of −30 dB (nominal EM energy remaining due to numerical noise in the calculation).

A simulated frequency sweep was initially used to determine the tuning frequency of each coil, and subsequent steady-state simulations were run using continuous wave radiation at resonant frequency. In the initial phantom simulations, the coils were matched by adjusting the resistance of dipole drives to minimise reflection. For body simulations, fixed input power and matching were used as is consistent with the approach taken in vivo. The simulated electric (E) and magnetic (B) fields for each transmit element were imported into Matlab R2018b (MathWorks, MA, USA) along with the S-matrices and used to calculate SAR_{10g}, B_1^+ and noise correlation matrices where required.

2.1 | SAR estimates

The 10 g averaged specific absorption rate (SAR_{10g}) was calculated for each voxel by first generating 10 g averaged Q matrices from the simulated E fields of each dipole element (8 × 8 matrix per voxel) as follows[16]:

$$\mathbf{Q_{10g}} = \frac{1}{m}\sum_{n=1}^{m}\frac{\sigma_n}{2\rho_n}\cdot\tilde{\boldsymbol{E}}_n^{\dagger}\cdot\tilde{\boldsymbol{E}}_n, \tag{1}$$

where m is the total number of voxels included within a 10 g cube of tissue centred on the voxel of interest; n is the index of each voxel within that volume; σ_n is tissue conductivity in each voxel; ρ_n is tissue density in each voxel; and $\tilde{\boldsymbol{E}}_n$ is the 3 × 8 matrix of the simulated electric field sensitivity components (x, y and z) from each dipole element in each voxel (the superscript † denotes the conjugate transpose). Previous studies have reduced computational demand by employing virtual observation points (VOPs)[23]; however, in this study, every voxel was included to give a complete representation of the image space. The Q_{10g} averaging space was determined by first growing cubic volumes to find the largest volume that included 10 g or less of tissue and then linearly interpolating an extra layer of voxels to make 10 g mass in total.[24] In line with previous work, volumes that included more than 20% air were excluded from calculations.[16]

From the Q_{10g}, the SAR_{10g} was calculated as follows:

$$SAR_{10g} = \boldsymbol{I}^{\dagger}\cdot\mathbf{Q_{10g}}\cdot\boldsymbol{I}, \tag{2}$$

where $\boldsymbol{I}$ is the 1 × 8 complex matrix representing the amplitude weighting and phase of the drive for each dipole element. As Equation (2) shows, for equally weighted input powers, the final SAR_{10g} in each voxel will depend only upon the phase settings for the eight dipole coils. Therefore, to assess the variability in SAR_{10g} for a coil operating at a maximum operational power limit, all amplitudes were weighted equally and scaled to 1 W

per channel, and SAR_{10g} values were calculated for 100,000 randomised phase settings (hence SAR_{10g} represents energy deposition for a 1 W per channel input power). Histograms and boxplots of the maximum SAR_{10g} values across all phase settings were created for visual comparisons.

To determine the worst-case scenario SAR_{10g} ($wocSAR_{10g}$) for a given set-up (i.e., the greatest possible maximum SAR_{10g} for any phase setting, across the whole simulated body), an iterative trigonometric maximisation algorithm[25] was applied with a convergence of 10^{-6} W kg^{-1}. Regions of the body with high energy deposition were illustrated by generating maximum intensity projections across all 100,000 phase settings of slices containing SAR_{10g} values greater than 90% of the $wocSAR_{10g}$ ($MIP_{90\%}$).

Calculations were performed using high-performance computing resources with 4720 cores and 31 TB RAM available in total. Calculations of SAR across the 100,000 random phase settings were run in parallel processing on 12 processors and took between 1 and 2 h to complete per simulation.

2.2 | RF coil model

A simplified simulation of an eight-channel, meandered dipole, parallel transmit coil (Figure 1)[20] was developed by modelling it as a single wire dipole electrically lengthened using inductors (75 nH, 2 mm either side of a central voltage source). Figure 2 compares the E fields and noise correlation matrices between the full and simplified coil models in a simulated muscle block phantom; a comparison of the corresponding maximum SAR_{10g} values is shown in Figure 3. Table 2 shows a comparison of the tuning frequencies as a single dipole is rotated with respect to the standard Cartesian mesh lines. Notably, the standard meshing methodology produces 'staircasing' (Figure 1C,D), which results in poor tuning at misaligned angles, whereas subcell meshing (i.e., XACT) and the simplified model allow for consistent tuning. The reduction in simulation time using the simplified coil model allowed for efficient modelling of the effects of coil variability, and as such, the simplified coil model was used throughout this study.

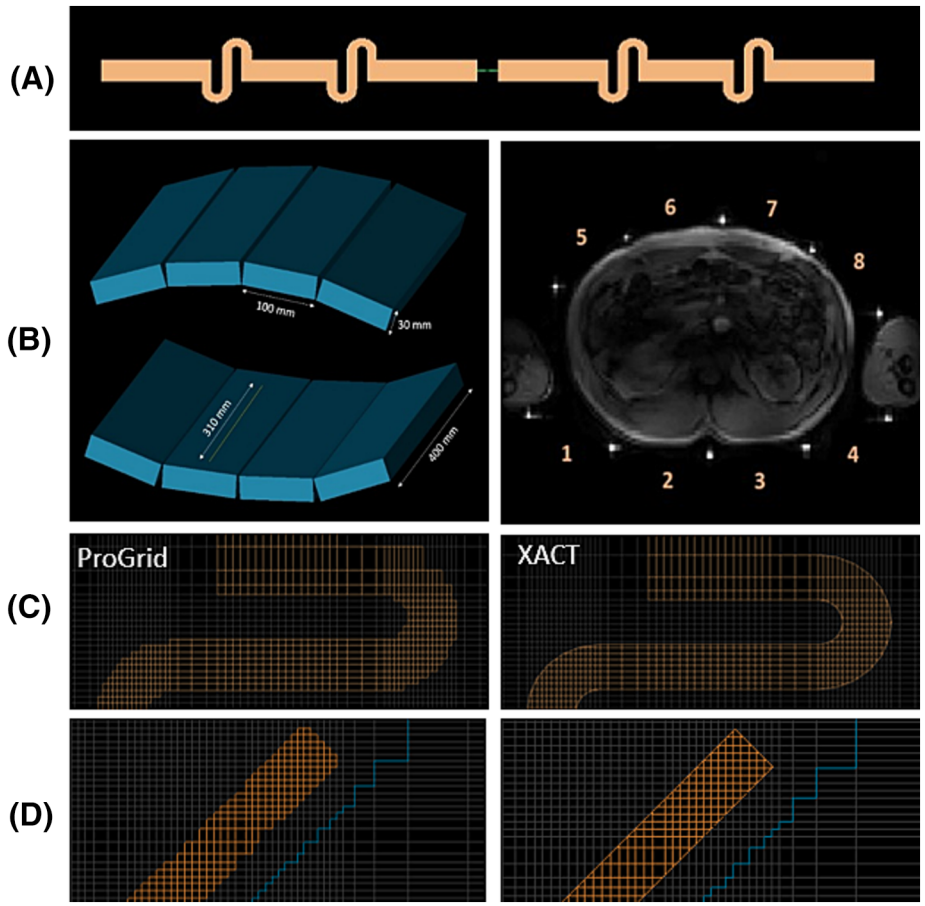

FIGURE 1 Electromagnetic simulation model of an eight-channel parallel transmit dipole coil. (A) Model of a single meandered dipole elements (length 300 mm, four meanders per element). (B) Anterior and posterior transmit element casings (400 × 100 × 30 mm^3) and 7 T MRI FFE scan showing fiducial markers attached between the transmit elements. (C and D) Comparison of meshing using standard Remcom's Cartesian (ProGrid) and subcellular conformal (XACT) meshing coronal and transverse slices, respectively.

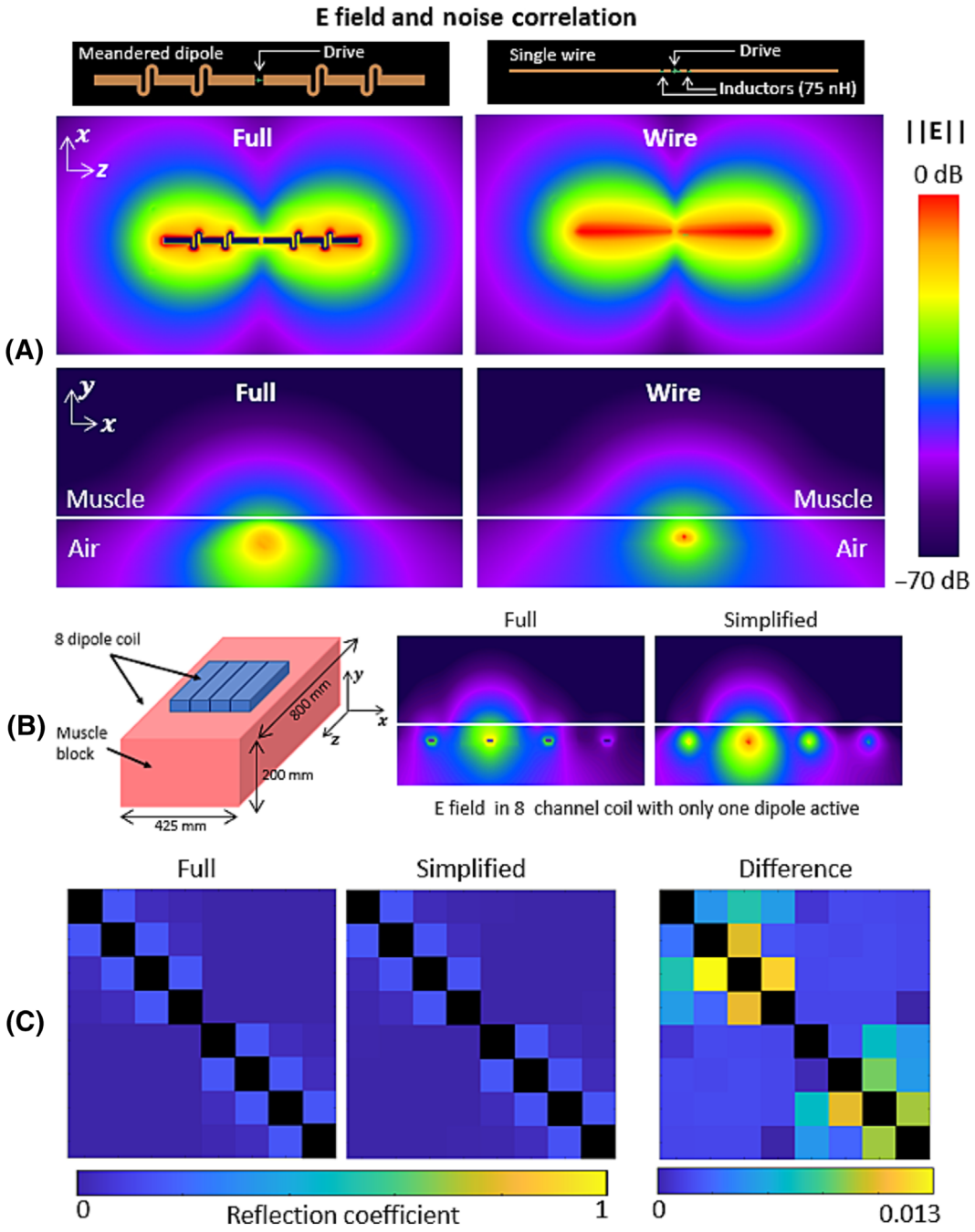

FIGURE 2 Comparison of $\|E\|$ field from full meandered dipole model and electrically lengthened single wire model for (A) A single dipole element with no adjacent elements in air (left) and when positioned directly below a muscle block (the insert shows the coil schematics); (B) A single dipole element driven as part of the eight-channel parallel transmit system, positioned directly next to a muscle block (as illustrated); (C) Noise correlation matrices for all eight dipole elements driven at 1 W, positioned directly next to a muscle block (illustrated in (B)).

2.3 | Body model

Individualised body models were generated from MR fat–water images acquired in 10 subjects (body mass index [BMI] = 25 ± 5 kg m^{-2}, six males and four females) during exhale breath-holds (3 T Philips Ingenia Scanner, two-point gradient echo images with fat and water reconstruction, TR = 5.0 ms, $TE_1/\Delta TE$ = 1.19/1.18 ms, flip angle = 3°, FOV = 560 × 300 × 560 mm^3, resolution = 1.3 × 1.3 × 5 mm^3). During scanning, a mock 7-T parallel transmit coil with eight fiducial markers was placed over the abdomen to indicate the position of dipole elements for later use in simulations.

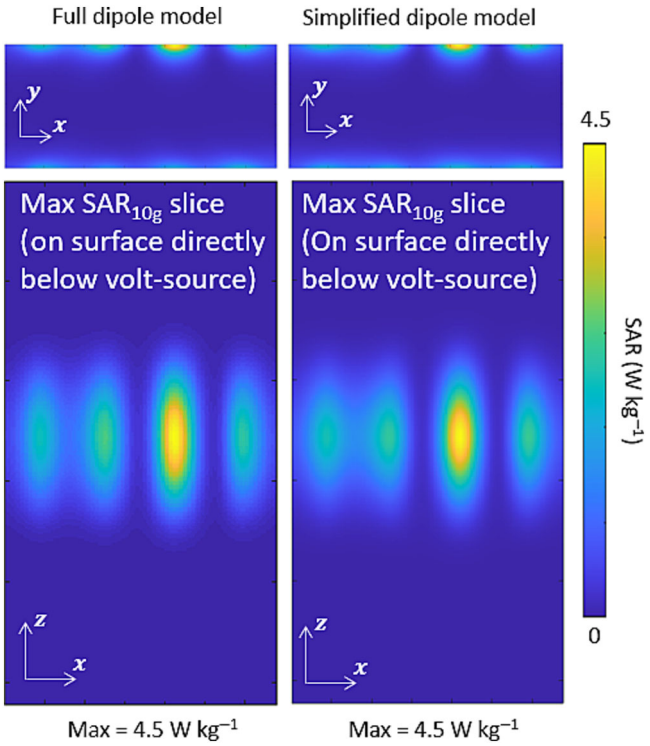

FIGURE 3 Comparison of simulated SAR_{10g} in the muscle block (illustrated in Figure 2B) for the eight-channel parallel transmit meandered dipole model (left) versus electrically lengthened wire model (right), each driven with a power of 1 W. Images are the slice with max SAR_{10g} across 100,000 random phase settings in two planes, as labelled. Max SAR_{10g} slice is at same position below the voltage source in both models (as seen in the figure, at the top of phantom under the second dipole element from the right). SAR_{10g}, 10 g averaged specific absorption rate.

TABLE 2 The effects of varying orientations with respect to the meshing grid for a full meandered dipole model with standard and XACT meshing and for a simplified wire dipole model. All simulations considered a dipole adjacent to a muscle cylinder (figure shows the angle of dipole on phantom where meshing gridlines stay horizontal and vertical).

Centre-slice cross section of cylindrical muscle phantom with single dipole rotated about axis

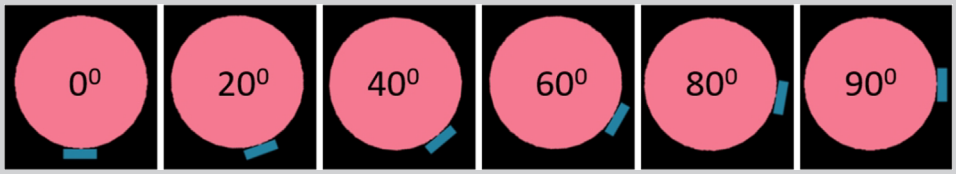

		Angle of single dipole with respect to meshing grid					
Model		**0°**	**20°**	**40°**	**60°**	**80°**	**90°**
Full standard	Tuning frequency (MHz)	360	900	1150	1150	940	360
	Simulation time (min)	35	21	15	10	11	35
	RAM required (MB)	437	420	511	452	395	440
Full XACT	Tuning frequency (MHz)	366	372	371	372	372	366
	Simulation time (min)	44	59	73	69	69	45
	RAM required (MB)	324	394	422	394	394	324
Simplified	Tuning frequency (MHz)	295	294	290	287	300	295
	Simulation time (min)	4	5	6	7	6	4
	RAM required (MB)	199	202	215	219	210	199

Abbreviation: XACT, Remcom's subcellular conformal meshing.

To assess the impact of respiration, subjects were immediately rescanned during an inhale breath-hold in the same scan session (three were unable to remain for the second inhale scan because of time constraints, resulting in $n = 7$ for the respiration analysis). Male participants had a BMI, muscle + organ volume percentage and fat volume percentage of 26 ± 6 kg m^{-2}, 59% ± 13% and 32% ± 14%, respectively; female participants had a BMI, muscle + organ volume percentage and fat volume percentage of 23 ± 3 kg m^{-2}, 52% ± 3% and 38% ± 3%, respectively.

The appropriate level of body truncation required for efficient simulations was investigated using the male heterogeneous computer body model available in the Remcom software. To determine the appropriate level of tissue segmentation required for efficient simulations, representative male and female models with matching BMI were chosen from the 10 models (both 24 kg m^{-2}) and segmented by tissue type. The EM properties were then assigned to each organ with varying degrees of precision (as shown in Table 1), and FDTD simulations were run to determine the SAR_{10g} across 100,000 random phase settings.

There was no impact on maximum SAR_{10g} for whole body versus upper body versus torso only, largely due to the position of maxima localised under the centre of the coil. Table 1 shows the comparison of simulations using varying degrees of tissue complexity. Notably, modelling the organs as muscle and/or bone as fat had minimal impact on the SAR values, whereas modelling skin as muscle or fat did. This is consistent with previous findings where reducing the complexity of tissue assignments to muscle, fat and lung produced results comparable with full tissue models,[26] allowing for efficient autosegmentation from fat–water images. Based on these results, the SAR variabilities in this study were investigated using torso-only body models with organs assigned as muscle; bones assigned as fat; and lungs and skin assigned according to their native EM properties (Table 1).

The EM tissue properties were fixed across all simulations based on previously determined values, and as such, it is possible that there are some intersubject variabilities not accounted for. However, this assumption is made in all SAR modelling and will therefore apply to all simulation data regardless of the model or tissue simplification used.

2.4 | SAR variability

2.4.1 | Variations in subject geometry

SAR_{10g} values were calculated in the 10 exhale models across 100,000 random phase settings. Histograms of maximum (max) SAR_{10g} were plotted and their variance calculated. Values of $wocSAR_{10g}$ were determined and $MIP_{90\%}$ maps generated. The relationship between $wocSAR_{10g}$ and BMI was analysed using linear regression, with the gradient, correlation coefficient and p values determined using the IBM SPSS Statistics software package version 24 (2016; IBM Corp., Armonk, NY, USA).

2.4.2 | Variability with respiration

SAR_{10g} values were calculated in the additional seven inhale models across 100,000 random phase settings and compared with the corresponding exhale models. Boxplots and $MIP_{90\%}$ maps were used to illustrate the change in the distribution of max SAR_{10g} between exhale and inhale.

2.4.3 | Variations in coil position

The representative male and female models (BMI matched, described above) were used to assess the effects of small variations in coil position. To mimic the effects of small coil displacements during scan set-up, five simulations were run on each model with the coil position displaced randomly over a 40 mm range in the right–left (R-L) direction and re-conformed to the shape of the body (foot–head direction remained constant). The maximum R-L and anterior–posterior (A-P) displacements are given in Table 3. Histograms of the maximum SAR_{10g} values for 1 W input power per channel across 100,000 random phase settings for each of the five positions were compared.

TABLE 3 Effects of repositioning the coil on local SAR_{10g} and the maximum displacement of the coil.

	Repositioning variability for 100,000 phase settings (W kg^{-1} mean ± standard deviation)			
	Average max SAR_{10g}	Standard deviation on max SAR_{10g}	Absolute max SAR_{10g}	Maximum displacement of coil (mm)
Male	2.00 ± 0.11	0.27 ± 0.03	3.00 ± 0.42	40 RL; 12 AP
Female	1.45 ± 0.04	0.23 ± 0.04	2.10 ± 0.20	40 RL; 22 AP

Abbreviations: AP, anterior–posterior; max SAR_{10g}, maximum 10 g averaged specific absorption rate; RL, right–left.

Unless otherwise stated, all values are quoted as mean ± standard deviation. The coefficient of variation (CV%) was calculated for both within- and between-subject variability.

3 | RESULTS

3.1 | Variations in subject geometry

Figure 4 shows the variation in the max SAR_{10g} at 1 W input per channel across 100,000 phase settings for the 10 scanned subjects. The max SAR_{10g} averaged across phase settings ranged from 1.4 to 2.3 W kg^{-1} with an overall average max SAR_{10g} across the 10 subjects of 1.8

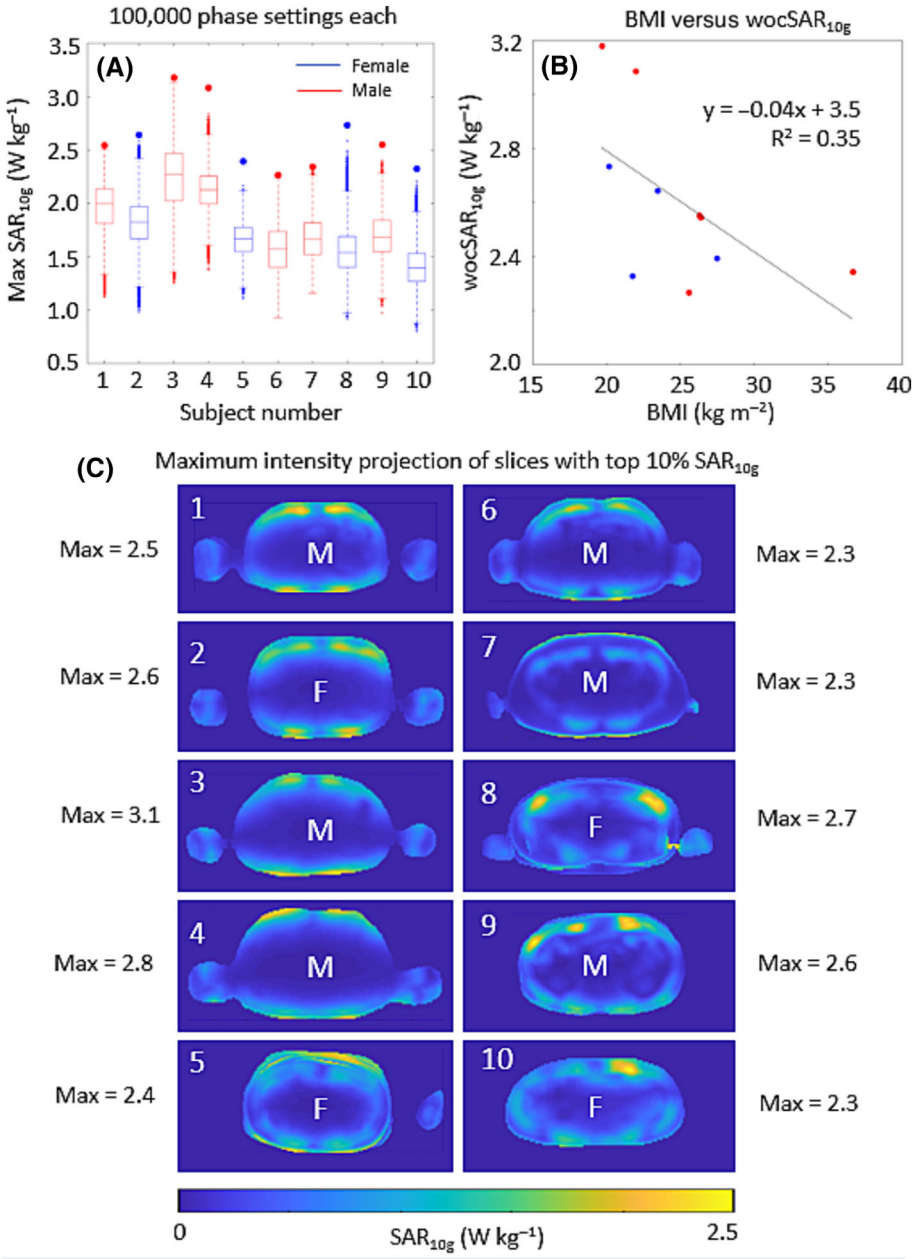

FIGURE 4 Comparison of SAR_{10g} in 10 subjects. (A) Boxplot of maximum (max) SAR_{10g} across 100,000 random phase settings (red and blue filled circles are for the worst-case scenario, $wocSAR_{10g}$). (B) BMI versus wocSAR10 g for each of the 10 subjects. (C) Individual top 10% SAR MIPs and maximum values across the 100,000 random phase variations. BMI, body mass index; MIP, maximum intensity projection; SAR, specific absorption rate; SAR_{10g}, 10 g averaged specific absorption rate.

± 0.3 W kg^{-1}. The average standard deviation due to variation in phase settings was 0.22 ± 0.05 W kg^{-1} (CV% = 12%). The wocSAR$_{10g}$ at 1 W input per channel averaged over the 10 subjects was 2.6 ± 0.3 W kg^{-1} (CV% = 12%), ranging from 2.3 to 3.2 W kg^{-1} (males: 2.7 ± 0.4 W kg^{-2}; females: 2.5 ± 0.2 W kg^{-2}). Values of wocSAR$_{10g}$ (filled circles in Figure 4) were in close agreement with the absolute maximum found over the random phase variations (indicated as a cross point on the boxplot in Figure 4).

The MIP$_{90\%}$ maps indicate that the hotspots always lay near the surface either in the skin close to the coil or in the muscle wall boundary. No hotspots were observed in internal organs (Figure 4C). A positive linear correlation was found between wocSAR$_{10g}$ and muscle + organ volume percentage (slope = 0.02, R = 0.7, p < 0.05) and a negative linear correlation between wocSAR$_{10g}$ and fat volume percentage (slope = −0.02, R = 0.8, $p \leq 0.01$). SAR$_{10g}$ was also correlated with BMI but did not reach significance (slope = −0.04, R = 0.6, p = 0.08; Figure 4B).

3.2 | Respiration

The effect of respiration phase on max SAR$_{10g}$ distributions across all subjects was minimal, as shown in Figure 5C. The subject-averaged wocSAR$_{10g}$ at 1 W input per channel was 2.6 ± 0.4 and 2.7 ± 0.4 W kg^{-1} for inhale and exhale simulations, respectively, with a maximum inhale–exhale difference in any subject of 0.2 W kg^{-1} for Subject 2. There was no consistent pattern of increase or decrease in max SAR$_{10g}$ due to respiration phase (Figure 5C). MIP$_{90\%}$ maps showed that hotspots remained near the surface (example in Figure 5B). The CV% attributable to the respiration phase was 4%.

3.3 | Coil repositioning

Table 3 and Figure 6 show the effects of small changes in coil position corresponding to realistic in vivo displacements. The wocSAR$_{10g}$ at 1 W input per channel across the five coil positions was 3.0 ± 0.4 and 2.1 ± 0.2 W kg^{-1} in the male and female models (CV% = 14% and CV% = 10%), respectively. There was no correlation between the magnitude of displacement and SAR$_{10g}$ in either the R-L or A-P directions.

The CV% values for the three sources of variation are summarised in Table 4.

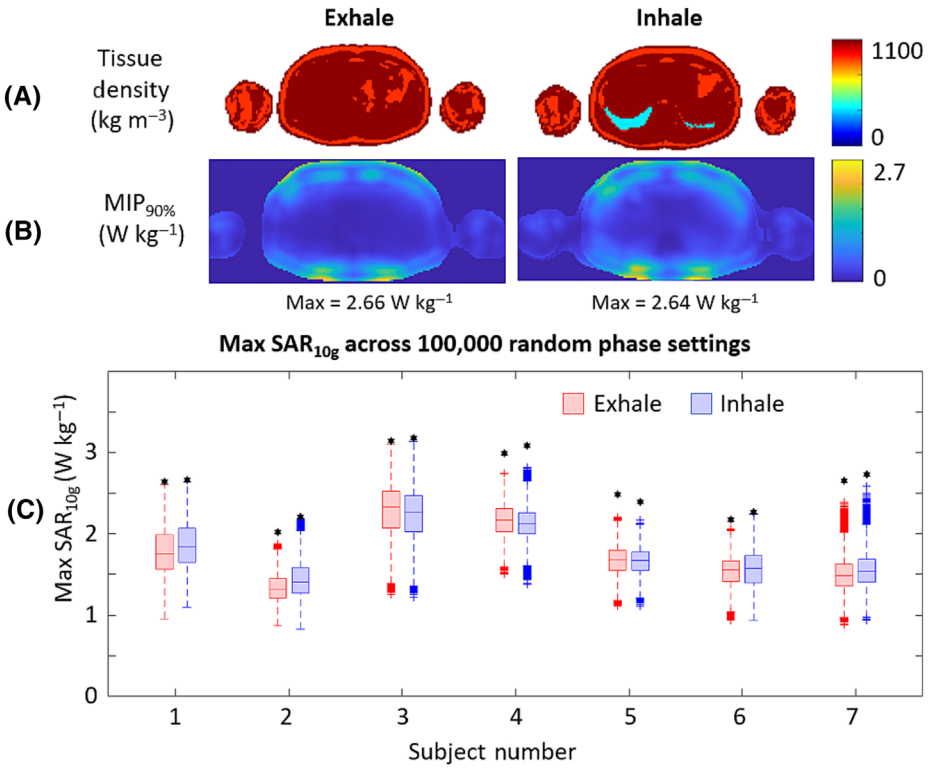

FIGURE 5 Example of simulations of a male body model during exhale (left) and inhale (right) showing (A) Tissue density maps (showing some lung on inhale). (B) Simulated local SAR$_{10g}$ maps. (C) Maximum (Max) SAR$_{10g}$ across 100,000 phase settings for inhale and exhale simulation (black asterisks represent the worst-case scenario SAR$_{10g}$). SAR$_{10g}$, 10 g averaged specific absorption rate.

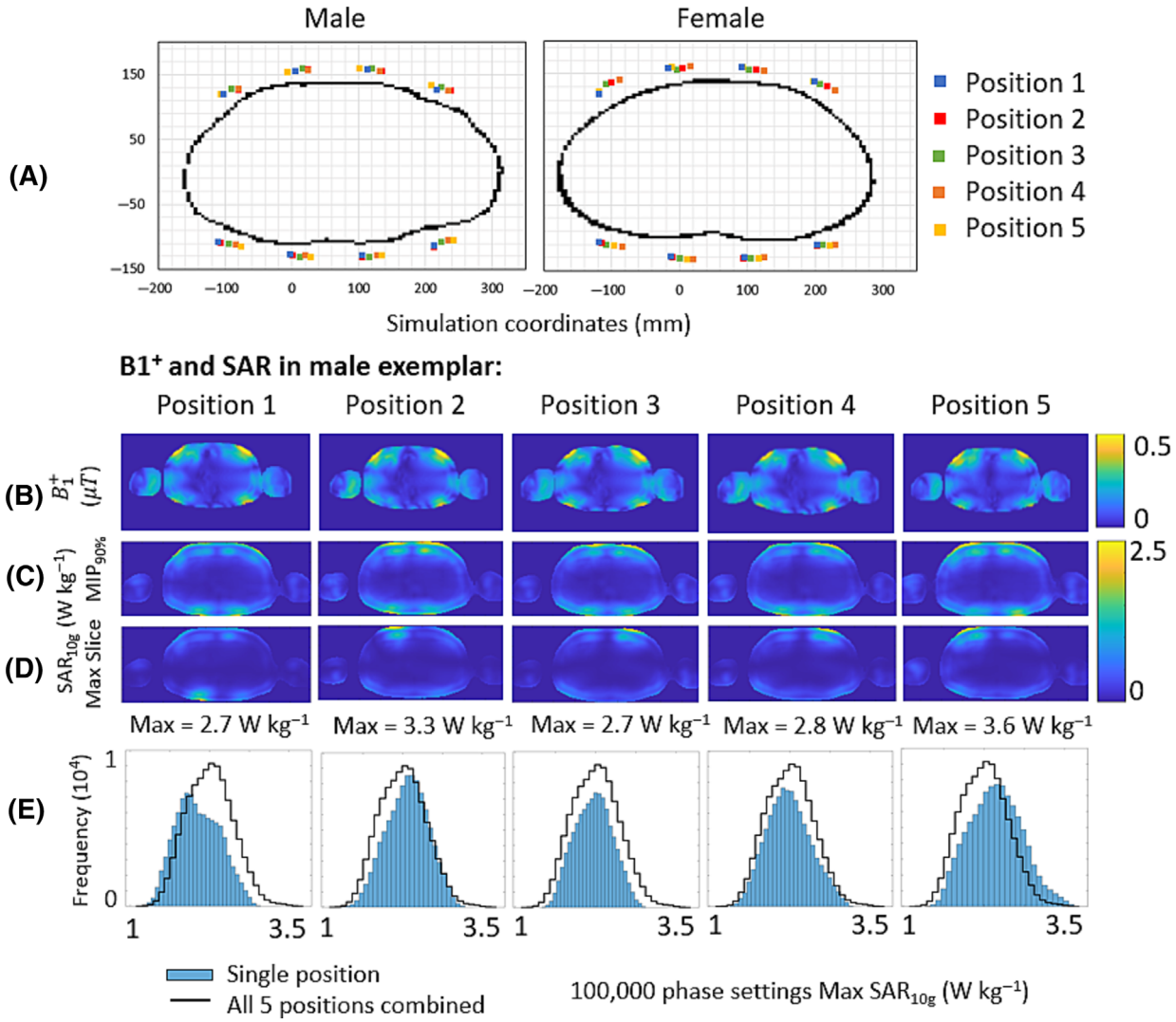

FIGURE 6 Comparison of five simulations of the representative body models with small variations in coil positions. (A) The five repositioned dipole displacements in the transverse plane; (B) B_1^+ in slice with maximum (max) SAR_{10g}; (C) Maximum intensity projection of slices with top 10% SAR_{10g}; (D) SAR_{10g} map for slice containing max SAR_{10g} value; and (E) Histograms of max SAR_{10g} for 100,000 random phase settings per subject overlaid on the combined histogram outline of all positions (the combined histogram is normalised to fit on the same scale as individual distributions). SAR_{10g}, 10 g averaged specific absorption rate.

TABLE 4 Comparison of CV% in SAR_{10g} for differing sources of variability. In the case of random phase settings, the SAR_{10g} value represents the average maximum (max) across all phase settings, and in the cases of intersubject, respiration and repositioning variability, the SAR_{10g} values represent the worst-case scenario (woc) SAR_{10g}.

Source of variability	SAR_{10g} (W kg^{-1})	CV%
100,000 random phase settings ($maxSAR_{10g}$)*	1.77	12%
Intersubject ($wocSAR_{10g}$)	2.61	12%
Respiration phase ($wocSAR_{10g}$)	2.64	4%
Repositioning of coil ($wocSAR_{10g}$)	2.55	12%

Abbreviations: CV%, coefficient of variation; SAR_{10g}, 10 g averaged specific absorption rate.
*CV% from random phase settings is based upon data from 10 subjects.

4 | DISCUSSION

This study explored the impact of differing sources of variability on SAR in parallel transmit abdominal imaging at 7 T. In contrast to parallel transmit MRI in the head, the use of flexible coils in abdominal imaging introduces multiple sources of variability that potentially play a role in accurately assessing SAR values and hence determining acceptable safety limits. By developing and testing a simplified coil and body model, multiple simulations could be run efficiently on in vivo generated models (using fat–water imaging to separate key tissues in the simplified model), and the effects of subject geometry, respiration phase, coil position and random phase variations could be assessed.

The variability between different body geometries (Figure 4) agreed with previous work[20] and reinforces the issue of high intersubject variability in local SAR_{10g} estimates. Notably, the variations between subjects were similar to the variation between different transmit phase settings for an individual subject's model (Table 4). Under normal operating modes, the power limits for local transmit body coils are determined by local SAR_{10g} values, which should not exceed 10 W kg^{-1} averaged over a 6-min period or 20 W kg^{-1} over a 10-s period (IEC guideline 60601-2-33 2022). In this study, the $wocSAR_{10g}$ across all subjects for any phase setting with 1 W input per channel was 3.1 W kg^{-1}, found near the surface of the body. This suggests that, for sequences with a RF duty cycle of up to even 50%, coils with a fixed maximum input power of 6 W per channel will still fall below SAR safety limits, even for the worst-case scenario (given repetition times < 20 s). For deep tissue scanning in the abdomen, increasing the coil's absolute safety power limits to generate sufficient B_1^+ becomes essential, and this study suggests that typically used limits of ~3 W per channel may be overly cautious. In addition, it is worth noting that this worst-case scenario is based on continuous wave RF at maximum power for the duration of transmission, which is rarely the case. In real-world scanning, other parameters are also considered when setting per channel power limits, such as maximum RF amplifier power outputs and instantaneous maximum SAR_{10g}. Even so, from a purely safety perspective, there appears to be scope to increase transmit power within current guidelines.

The relationship between fat volume percentage and SAR_{10g} indicates that subjects with less adipose tissue are more susceptible to higher energy deposition. Given that hotspots were normally observed in the muscle near the surface of the body, these correlations are likely to be due to subcutaneous adipose tissue varying the distance between the coil and abdominal muscle wall. Interestingly, the representative male and female models used in this study to investigate coil repositioning were BMI matched (24 kg m^{-2}) but exhibited differences in fat to muscle + organ ratios (male: 0.5; female: 0.7). This probably explains the large difference in $wocSAR_{10g}$ between the two models and suggests that internal abdominal features are the most relevant factor for safety considerations. These findings highlight the potential inadequacy of using a generic power limit that does not account for intersubject variability, with the $wocSAR_{10g}$ produced in subjects with less adipose tissue (where a lower B_1^+ may be sufficient for deep tissue scanning) limiting the power input in subjects with more adipose tissue (where a greater B_1^+ is required).

In contrast to intersubject variability, the effect of respiration on the distribution of max SAR_{10g} values across phase settings was minimal. This may be expected because the max SAR_{10g} values occurred at the surface away from lung–organ boundaries, particularly for the abdomen. By contrast, Schoen et al. found that respiration had a significant impact on 7-T parallel transmit cardiac imaging, with inhale increasing the potential maximum local SAR_{10g}.[21] This suggests that the target region for scanning is a relevant factor in assessing the energy absorption; for cardiac imaging, the effects of lung inflation need to be accounted for when designing scans and setting power limits, whereas for abdominal scanning, this study found no significant effect.

Importantly, this study found that realistic variations in simulated coil position had a significant impact on the max SAR_{10g}, exceeding the effects of respiration phases but comparable with intersubject variability (14% and 10% variability in $wocSAR_{10g}$ for coil repositioning in the male and female models, respectively; 13% variability in $wocSAR_{10g}$ across 10 subjects). Notably, this study only focused on displacements in the R-L direction, whereas potential repositioning inconsistencies can also occur in the F-H direction. While previous studies have considered the effects of varying driving phases and body types, EM simulations are usually only run for one coil position.[20,27] This may be more reasonable for parallel transmit systems with fixed coil geometries, for example, head coils, but is not appropriate for abdominal scanning with a wrap-around coil. Because the exact positioning of a wrap-around coil on the body is inevitably somewhat arbitrary and variable, variations in B_1^+ and local SAR_{10g} distributions with realistic coil repositioning or movement provide a practical limit on the uncertainty of results from all other simulations.

Ultimately, the safety concern in high-field parallel transmit imaging is tissue damage through excessive heating. While this is related to SAR, hence requiring accurate models, other factors may also come to bear. It is notable, for example, that in this study, SAR hotspots always occurred near the surface (see MIPs in Figure 4), where heating is more likely to be reduced through close proximity to air and the skin's thermoregulatory properties. Yet, it is these hotspots that dictate the power available to the coil and may present challenging limits on achieving effective B_1^+ for deep tissue imaging. While previous studies have explored the relationship between SAR and heating in the human head,[28] further work is needed to determine these heating effects with flexible abdominal coils.

Related to this, calculated SAR_{10g} values depend on the algorithm used for averaging and the inclusion or otherwise of voxels near the surface. While cubic region growing provides a practical and efficient solution for meshed simulations, it is difficult to interpret its applicability to real-life energy deposition. Additionally, averaging algorithms include a cut-off threshold to exclude volumes that contain a certain proportion of air, but there is a lack of consensus on how much is too much, ranging from 5% to 20%.[24] The current study used the most conservative value in this range to include all averaging volumes below 20% air. Further work should explore the effects of different SAR averaging approaches and the comparability with real-life energy deposition. This is particularly relevant in the skin and surface regions where large changes in conductivity

occur over small distances. If max SAR_{10g} can be predicted to always be near the dipoles at the surface, then it may be possible to focus simulations on those regions to allow more detailed modelling of these interfaces and to reduce computational demands and simulation time.

One limitation of this study is that SAR values were determined purely on the assumption of maximum power output per channel. This was to assess potential worse-case scenarios to provide an absolute upper bound on abdominal scanning. By employing RF shimming or novel pulse designs, the simulated SAR can be significantly reduced by reducing power from coils when unnecessary. Further work should explore the implications of this for increasing the per-channel power output limits further, therefore improving deep tissue scanning.

5 | CONCLUSION

This study has shown that, in abdominal 7-T MRI using a fractionated dipole array coil, max SAR_{10g} always occurs near the surface. This suggests that there is an opportunity to focus estimates of SAR_{10g} only in a small region near the expected hotspots to reduce computational demands and simulation time further. This study found that $wocSAR_{10g}$ was inversely related to fat volume and BMI and that respiration had a minimal impact on SAR distribution and maximum SAR_{10g} values, whereas the variation in coil position on a single subject produced variations that were comparable with intersubject variability. This suggests that appropriate uncertainty bounds must be placed on individualised estimates of SAR_{10g} to take account of possible variations in coil position; indeed, in some situations, there may be no value in producing individualised SAR simulations because variations in coil position are likely to produce variations in SAR that are comparable with intersubject variability.

CONFLICT OF INTEREST STATEMENT

There are no conflicts of interest to declare.

ORCID

Stephen Bawden https://orcid.org/0000-0002-5157-3269

REFERENCES

1. Laader A, Beiderwellen K, Kraff O, et al. 1.5 versus 3 versus 7 Tesla in abdominal MRI: a comparative study. *PLoS ONE*. 2017;12(11):e0187528. doi:10.1371/journal.pone.0187528
2. Vaughan JT, Garwood M, Collins CM, et al. 7T vs. 4T: RF power, homogeneity, and signal-to-noise comparison in head images. *Magn Reson Med*. 2001;46(1):24-30. doi:10.1002/mrm.1156
3. Padormo F, Beqiri A, Hajnal JV, Malik SJ. Parallel transmission for ultrahigh-field imaging. *NMR Biomed*. 2016;29(9):1145-1161. doi:10.1002/nbm.3313
4. Graessl A, Renz W, Hezel F, et al. Modular 32-channel transceiver coil array for cardiac MRI at 7.0T. *Magn Reson Med*. 2014;72(1):276-290. doi:10.1002/mrm.24903
5. Thalhammer C, Renz W, Winter L, et al. Two-dimensional sixteen channel transmit/receive coil array for cardiac MRI at 7.0 T: design, evaluation, and application. *J Magn Reson Imaging*. 2012;36(4):847-857. doi:10.1002/jmri.23724
6. Snyder CJ, DelaBarre L, Moeller S, et al. Comparison between eight- and sixteen-channel TEM transceive arrays for body imaging at 7 T. *Magn Reson Med*. 2012;67(4):954-964. doi:10.1002/mrm.23070
7. Raaijmakers AJE, Italiaander M, Voogt IJ, et al. The fractionated dipole antenna: a new antenna for body imaging at 7 Tesla. *Magn Reson Med*. 2016;75(3):1366-1374. doi:10.1002/mrm.25596
8. Zivkovic I, de Castro CA, Webb A. Design and characterization of an eight-element passively fed meander-dipole array with improved specific absorption rate efficiency for 7 T body imaging. *NMR Biomed*. 2019;32(8):e4106. doi:10.1002/nbm.4106
9. Raaijmakers AJE, Ipek O, Klomp DWJ, et al. Design of a radiative surface coil array element at 7 T: the single-side adapted dipole antenna. *Magn Reson Med*. 2011;66(5):1488-1497. doi:10.1002/mrm.22886
10. Wolf S, Diehl D, Gebhardt M, Mallow J, Speck O. SAR simulations for high-field MRI: how much detail, effort, and accuracy is needed? *Magn Reson Med*. 2013;69(4):1157-1168. doi:10.1002/mrm.24329
11. Neufeld E, Gosselin MC, Murbach M, Christ A, Cabot E, Kuster N. Analysis of the local worst-case SAR exposure caused by an MRI multi-transmit body coil in anatomical models of the human body. *Phys Med Biol*. 2011;56(15):4649-4659. doi:10.1088/0031-9155/56/15/002
12. IEC. SAR compliance. 2010. pp. 60601.
13. Center for Devices Health and Radiological, U.S.F.A.D.A. Criteria for significant risk investigation of magnetic resonance diagnostic devices. 2014.
14. Moyher SE, Vigneron DB, Nelson SJ. Surface coil MR-imaging of the human brain with an analytic reception profile correction. *J Magn Reson Imaging*. 1995;5(2):139-144. doi:10.1002/jmri.1880050204
15. Su T, Mittra R, Yu W, Wiart J. Calculation of SAR using FDTD sub-domain approach. In *IEEE/ACES International Conference on Wireless Communications and Applied Computational Electromagnetics*. 2005.
16. Graesslin I, Homann H, Biederer S, et al. A specific absorption rate prediction concept for parallel transmission MR. *Magn Reson Med*. 2012;68(5):1664-1674. doi:10.1002/mrm.24138
17. Beggs JH, Luebbers RJ, Yee KS, Kunz KS. Finite-difference time-domain implementation of surface impedance boundary-conditions. *EEE Trans Antennas Propag*. 1992;40(1):49-56. doi:10.1109/8.123352
18. Seifert F, Wübbeler G, Junge S, Ittermann B, Rinneberg H. Patient safety concept for multichannel transmit coils. *J Magn Reson Imaging*. 2007;26(5):1315-1321. doi:10.1002/jmri.21149

19. Homann H, Graesslin I, Eggers H, et al. Local SAR management by RF shimming: a simulation study with multiple human body models. *Magn Reson Mater Phys Biol Med*. 2012;25(3):193-204. doi:10.1007/s10334-011-0281-8
20. Meliado EF, van den Berg CAT, Luijten PR, Raaijmakers AJE. Intersubject specific absorption rate variability analysis through construction of 23 realistic body models for prostate imaging at 7T. *Magn Reson Med*. 2019;81(3):2106-2119. doi:10.1002/mrm.27518
21. Schoen N, Seifert F, Petzold J, et al. The impact of respiratory motion on electromagnetic fields and specific absorption rate in cardiac imaging at 7T. *Magn Reson Med*. 2022;88(6):2645-2661. doi:10.1002/mrm.29402
22. Luebbers RJ, Kunz KS, Chamberlin KA. An interactive demonstration of electromagnetic-wave propagation using time-domain finite-differences. *IEEE Trans Educ*. 1990;33(1):60-68. doi:10.1109/13.53628
23. Eichfelder G, Gebhardt M. Local specific absorption rate control for parallel transmission by virtual observation points. *Magn Reson Med*. 2011;66(5):1468-1476. doi:10.1002/mrm.22927
24. Caputa K, Okoniewski M, Stuchly MA. An algorithm for computations of the power deposition in human tissue. *IEEE Antennas Propag Mag*. 1999;41(4):102-107. doi:10.1109/74.789742
25. Meliado EF, Sbrizzi A, van den Berg CAT, Luijten PR, Raaijmakers AJE. Real-time assessment of potential peak local specific absorption rate value without phase monitoring: Trigonometric maximization method for worst-case local specific absorption rate determination. *Magn Reson Med*. 2021;85(6):3420-3433. doi:10.1002/mrm.28635
26. Homann H, Börnert P, Eggers H, Nehrke K, Dössel O, Graesslin I. Toward individualized SAR models and in vivo validation. *Magn Reson Med*. 2011;66(6):1767-1776. doi:10.1002/mrm.22948
27. de Greef M, Ipek O, Raaijmakers AJE, Crezee J, van den Berg CAT. Specific absorption rate intersubject variability in 7T parallel transmit MRI of the head. *Magn Reson Med*. 2013;69(5):1476-1485. doi:10.1002/mrm.24378
28. Collins CM, Liu W, Wang J, et al. Temperature and SAR calculations for a human head within volume and surface coils at 64 and 300 MHz. *J Magn Reson Imaging*. 2004;19(5):650-656. doi:10.1002/jmri.20041

How to cite this article: Doran E, Naim I, Bowtell R, Gowland PA, Glover PM, Bawden S. The impact of variations in subject geometry, respiration and coil repositioning on the specific absorption rate in parallel transmit abdominal imaging at 7 T. *NMR in Biomedicine*. 2023; e5032. doi:10.1002/nbm.5032